Parallel astrocyte calcium signaling modulates olfactory bulb responses

Kevin Ung[a], **Burak Tepe**[a], **Brandon Pekarek**[b], **Benjamin R. Arenkiel**[a,b,e,*], **Benjamin Deneen**[a,c,d,*]

[a]Program in Developmental Biology, Houston, TX 77030, USA

[b]Department of Molecular and Human Genetics, Houston, TX 77030, USA

[c]Center for Cell and Gene Therapy, Houston, TX 77030, USA

[d]Department of Neurosurgery, Baylor College of Medicine, Houston, TX 77030, USA

[e]Jan and Dan Duncan Neurological Research Institute at Texas Children's Hospital, Houston, TX 77030, USA

Abstract

Astrocytes are the most abundant glial cell in the CNS. They modulate synaptic function through a variety of mechanisms, and yet remain relatively understudied with respect to overall neuronal circuit function. Exploiting the tractability of the mouse olfactory system, we manipulated astrocyte activity and examined how astrocytes modulate olfactory bulb responses. Towards this, we genetically targeted both astrocytes and neurons for *in vivo* wide-field imaging of Ca^{2+} responses to odor stimuli. We found that astrocytes exhibited odor-response maps that overlap with excitatory neuronal activity. By manipulating Ca^{2+} activity in astrocytes using chemical genetics we found that odor-evoked neuronal activity was reciprocally affected, suggesting that astrocyte activation inhibits neuronal odor responses. Subsequently, behavioral experiments revealed that astrocyte manipulations affect both odor detection threshold and discrimination, suggesting that astrocytes play an active role in olfactory sensory processing circuits. Together, these studies show that astrocyte calcium signaling contributes to olfactory behavior through modulation of sensory circuits.

Graphical Abstract

*Correspondence: Benjamin Deneen, Ph.D, Center for Cell and Gene Therapy, Baylor College of Medicine, Houston, TX 77030, USA, Tel: 713.798.7897, deneen@bcm.edu; Benjamin R. Arenkiel, Ph.D, Dept. of Molecular & Human Genetics, Jan and Dan Duncan Neurological Research Institute, Baylor College of Medicine, Houston, TX 77030, USA, Tel: 713.798.1960, FAX: 832.825.1240, arenkiel@bcm.edu.

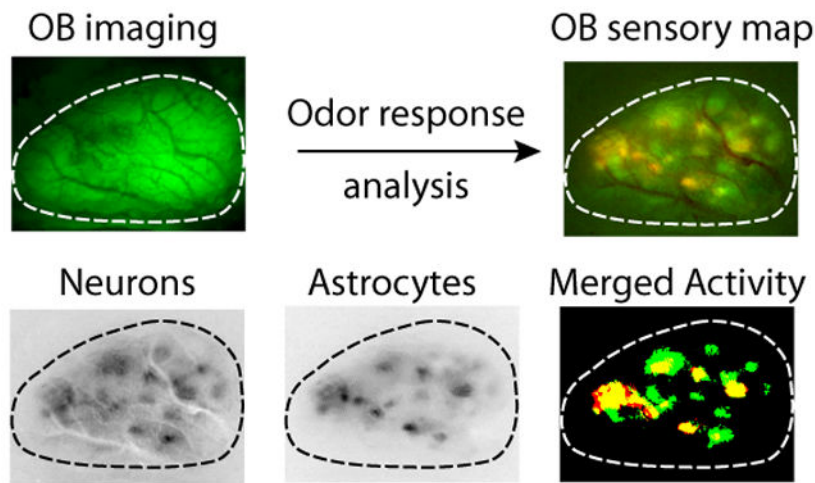OB imaging → Odor response analysis → OB sensory map

Neurons   Astrocytes   Merged Activity

Keywords

astrocyte; calcium; olfaction; DREADD; circuit; neuron-astrocyte interactions

Introduction

In the CNS, sensory systems are often associated with topographical representations, or sensory maps. Sensory maps are established via multiple mechanisms, including molecular cues, spontaneous or sensory-dependent remodeling, and cellular refinement (Cang & Feldheim, 2013). Initially, sensory maps are broad and overlapping. Through critical periods during development, activity-dependent refinement sculpts these diffuse patterns into discrete segments of sensory circuits. Although our understanding of the functional relevance of sensory maps remains incomplete, the general thought is that sensory maps align specific domains of CNS tissue with input from the external world to preserve and relay information in a structured, neuron-dependent manner.

Glial cells are important regulators of proper neural development and circuit function (Freeman, 2006; Lemke, 2002; Ma, Ming, & Song, 2005). Notably, they play crucial roles in the development, function, and adaptation of neuronal circuits. Astrocytes, the most abundant glial cells in the brain, are characterized by an elaborate bushy morphology, and low-resistance passive membrane properties (Sofroniew & Vinters, 2010). Classically, astrocytes have been considered primarily a support cell, by providing metabolic balance to neurons through astrocyte-neuron lactate shuttling (Magistretti, 2006), potassium buffering (Amédée, Robert, & Coles, 1997; Bordey, Hablitz, & Sontheimer, 2000; Higashimori & Sontheimer, 2007; Newman et al., 1995), neurovascular coupling (Haydon & Carmignoto, 2006; Otsu et al., 2014), glutamate recycling (Bergles & Jahr, 1998; Schousboe, 2018), and regulating extracellular osmotic space (Vargova & Sykova, 2009). More recently, astrocyte signaling has been recognized as an active process in neuromodulation through both direct and indirect signaling mechanisms (Eroglu & Barres, 2010; Hanson et al., 2015). Astrocytes do not display action potential-dependent signaling; instead, astrocyte signaling is thought to be mediated through intracellular calcium. Astrocyte calcium as a possible mediator of

neuronal signaling has been an area of intense focus since astrocyte calcium signals were discovered. Indeed, astrocyte calcium signaling has only recently been linked to an ever increasing range of cell-intrinsic functions that affect neuronal signaling (Fields, Woo, & Basser, 2015; Robel & Sontheimer, 2015; Weiss, Melom, Ormerod, Zhang, & Littleton, 2019). Despite this, the full extent to which astrocyte signaling governs activity-dependent function and refinement of neuronal sensory maps have yet to be explored.

Here we sought to both investigate how astrocyte-to-neuron communication influences the integration of sensory information, and query whether sensory input-driven activity in astrocytes leads to modulation of sensory circuits. Towards this, we measured *in vivo* astrocytic responses to olfactory stimulation, and *in vivo* neuronal responses to olfactory stimuli while we selectively manipulated astrocyte activity in the mouse olfactory bulb (OB). As a readout of olfactory stimulation, we directly monitored the mitral and tufted cells (M/Ts), the main excitatory neuron population in the OB that relays odor information to the piriform cortex. We found that astrocytes are activated in spatially defined domains that overlap with M/T activity, and directly participate in sensory information processing. Using chemical genetic approaches, we found that increasing astrocyte Ca^{2+} activity caused a decrease in M/T odor responses, while lowering astrocyte Ca^{2+} activity led to elevated neuronal odor responses. Finally, *in vivo* manipulations of astrocyte activity affected olfactory perception in mice by changing odor detection thresholds, further substantiating astrocytes as integral players in olfactory information processing.

Materials and Methods

Experimental Subjects

Experiments and care of adult, virgin male and female *Aldh1L1-Cre* or *Aldh1L1-Cre; Thy1-GCaMP3* mice backcrossed into a C57BL/6J strain (n = 31 male and 33 female mice) were conducted according to the BCM IACUC approved protocol in accordance with the guidelines set by the National Institutes of Health and the Guide for the Care and Use of Laboratory Animals. Sex was not considered a biological variable. The mice were housed in an animal facility separated by sex on a 12-hr light/dark cycle. The experimental tests were carried out during the light phase. Mouse chow and water were available ad libitum unless otherwise stated. One animal was excluded for failing to successfully learn the behavioral task and one data point in fluorescent kinetics was excluded as an outlier using the Grubbs's test for identifying outliers.

Stereotaxic microinjection of adeno-associated viruses

Stereotaxic injections into the mouse olfactory bulb were performed as previously described (Quast et al., 2017). Surgical procedures were conducted under general anesthesia using Ketamine/dexdormitor induction (75 mg/kg and 0.5 mg/kg respectively) and maintained under volatile isoflurane inhalation (maintenance at 1%-2.5% vol/vol). Depth of anesthesia was monitored continuously and adjusted when necessary. Following induction of anesthesia, mice were fixed within a stereotaxic frame with their heads secured by blunt ear bars and their noses placed into an anesthesia and ventilation system. They were administered 5 mg/kg of meloxicam subcutaneously prior to surgery. The surgical site was

then cleaned three times with 10% iodine and 70% isopropanol (vol/vol). Skin incisions were made, followed by craniotomies of 2-3 mm in diameter above the olfactory bulb using a small steel burr (Hager & Meisinger GmbH) powered by a high-speed drill (Vector Mega Torque). Saline (0.9%) was applied onto the skull to reduce heating caused by drilling. Bilateral viral injections into the olfactory bulb were carried out by using a stereotaxic apparatus (Leica Biosystems) to guide the placement (from bregma: ML, ±0.9 mm; AP, 3.82 mm; and 0.65 mm down from the surface of the OB) of beveled glass pipettes (3-000-203-G/X, Drummond Scientific Company). Adeno-associated viruses (AAVs) were injected by using a syringe pump (Nanoject II, Drummond Scientific Company) at a rate of 69 nL/s at 25 s intervals 10 times to obtain uniform labeling of astrocytes. Glass pipettes were left in place for at least 5 minutes prior to slow withdrawal. Surgical wounds were closed with surgical nylon monofilament sutures. Mice were allowed to recover overnight in cages placed partially on a low-voltage heating pad. Meloxicam was administered once a day for 3 days after surgery. Virus injected mice were euthanized two to three weeks post-surgery after *in vivo* widefield imaging, or prior to live slice imaging or perfusion for immunohistochemistry. AAVs serotype 2/9 encoding flexed-hM3D-mCherry, flexed-hM4D-mCherry, or flexed-jRCaMP1a under the GFAP promoter were cloned and packaged (~2.5 × 10^{12} viral particles/mL) in house.

Immunohistochemistry and confocal imaging

For confocal imaging, animals were deeply anesthetized using isoflurane, followed by intracardial perfusion of phosphate buffered saline (PBS) and 4% PFA in PBS (pH 7.35). Brains were dissected, postfixed in 4% PFA at 4°C for 1 hour before cryoprotection in 20% sucrose overnight. Olfactory bulbs were embedded in OCT before coronally sectioning at 40 μm using a cryostat (CM1860, Leica). Before immunostaining, sections were rinsed once in PBS and incubated 1 hr at RT in a blocking buffer (0.3% Triton X-100 and 10% normal goat serum in PBS). For immunolabeling, sections were incubated with primary antibodies diluted in blocking buffer for 16-18 hr at 4°C on an orbital shaker. After rinsing at RT with PBS with 0.3% Triton-X (PBS-T) 3x for 15 min each, sections were incubated on an orbital shaker with fluorescent dye-conjugated secondary antibodies diluted in blocking buffer for 2 hr at RT. After rinsing 3x in PBS-T, sections were mounted on charged glass-slides and coverslipped in Fluoromount-G (Cat# 0100-01, SouthernBiotech). Primary antibodies used: rabbit anti-GFAP (DAKO, Z0334, 1:1000, RRID: AB_2811722), rabbit anti-Tbx21 (gift from Mitsui lab, 1:500), rabbit anti-TH (Millipore, Ab152, 1:2000, RRID: AB_390204), mouse anti-calretitin (Millipore, MAB1568, 1:1500, RRID: AB_94259), and mouse anti-parvalbumin (Millipore, MAB1572, 1:3000, RRID: AB_2174013). Secondary antibodies used were (raised in goat): anti-rabbit Alexa-488 (Thermofisher, A10040, 1:500, RRID: AB_2534016) and anti-mouse Alexa-488 (Thermofisher, A11001, 1:500, RRID: AB_2534069). Confocal images were acquired using a Leica TCS SPE confocal microscope with a 20x objective (Leica) and the pinhole set to 1 airy unit. Images represent maximum intensity projections of image stacks with a step size of 0.5 μm.

Calcium imaging

In vivo wide-field calcium imaging was performed in anesthetized (urethane, 1.2 μm/kg) head-fixed animals (8-14 weeks old) through thinned skulls 2 to 3 weeks after viral

injection. Animals were kept warm with a portable heating pad and a local anesthetic (bupivicane, 0.5%) was applied to the incision areas. Sensory evoked responses were acquired with a Leica M205FA microscope at 6x magnification, using a GFP or RFP filter set sequentially, and a Leica FL6000 fluorescence light source. Optical signals were recorded for 10 s per trial at 464×346 pixel resolution. A CCD camera (DFC360 FX, Leica) captured images at a frame rate of 10 Hz, and videos were digitized at 12 bits using Leica Application Suite software. Odorants were presented using a custom-made olfactometer (stimulus duration, 3 s) and were presented as ~1% saturated vapor, and adjusted for vapor pressure. Separate lines for each odorant were used to prevent cross contamination. The odors were presented in a random order with at least three trials per odorant at interstimulus intervals 60 s.

Olfactory associative training and odor detection threshold assays

Mice received viral injections prior to training. Mice were water-restricted to no less than 85% of their baseline weight beginning 2 d before preliminary training. Water was restricted to 40 mL per kg, per day during the restriction period. For the training group, mice were trained using a Go/NoGo paradigm in a behavioral chamber with infrared nose pokes (Med Associates Inc.). All mice were first trained to poke their nose into the odor port for at least 300 ms, before moving to the side water port to retrieve water reward within 5 s. After preliminary training sessions (~30 - 60 min/d for ~5 - 6 d), mice were trained to respond to the Go odor stimulus (S+) (1% anisole in mineral oil) by moving to the water port for a reward, and were trained to respond to the NoGo odor stimulus (1% acetophenone in mineral oil) by refraining from poking into reward ports and starting a new trial. Mice needed to sample the odors for at least 100 ms before responding, and were required to respond within 5 s after odor port poking. False positives (incorrect NoGo response) caused a 4 s timeout punishment. Go and NoGo stimuli were presented to the mice in random sequences during training. Mice were trained for 20 trials per block and ~20 blocks per day. After 3 - 6 days of odor training, mice performing at over 80% accuracy were considered trained. For assaying odor detection threshold, mice were tested with dilutions of Go and NoGo odor stimuli in descending order after training.

Quantification and Statistical Analysis

For wide-field calcium imaging, all data analysis was performed with custom written MATLAB (Matlab, Natick, MA, RRID: SCR_001622) scripts and processed in FIJI (RRID: SCR_002285). Initial data processing included averaging trials and visually aligning the region of interest (dorsal olfactory bulb). F maps were created by temporally averaging the entire 3 s odor stimulation period, and subtracting the temporal average of 2 s immediately preceding odor onset. F/F maps were additionally normalized by the first five frames of the averaged trial. Photobleach correction was performed using a simple ratio method within FIJI. Binary thresholded maps were generated using an automated maximum entropy threshold in FIJI, and overlap was calculated using a custom written MATLAB script to quantify the percent of activated neuronal domains that also contained activated astrocyte domains. For quantification, ROIs approximately the size of a glomerulus were set over activated regions with at least 3 ROIs per odorant. The values for these ROIs were averaged together to generate a response trace per odorant trial per animal as a technical repeat. The

technical repeats for an odor were averaged together to generate a representative response for that given odor.

Data are expressed as ± standard deviation. Statistical analysis of the data was performed in GraphPad Prism Version 6.0e (GraphPad Software, La Jolla, CA, USA, RRID: SCR_002798). Two-way repeated measures ANOVA with Sidak's multiple comparison correction was used for widefield calcium imaging. Unpaired Student's T-test analysis was used for fluorescent kinetics. For depicting behavioral data, dot plots were used with error bars representing standard deviation. Paired T-test was used for behavioral data. Differences were considered significant at $p < 0.05$.

Data and software availability

All scripts are available upon request.

Results

Genetic labeling of olfactory bulb astrocytes

To selectively target astrocytes in the olfactory bulb, we implemented conditional viral genetic methods by injecting conditional Cre-dependent ("flex") viruses harboring reporter constructs into the OBs of *Aldh1L1-Cre*^{+/−} mice (RRID: IMSR_JAX:023748) (Figure 1A). Given that *Aldh1L1* is selectively expressed in CNS astrocytes (Cahoy et al., 2008), this strategy affords cell type-specific transgene expression exclusively in astrocytes. Also, conditional viral approaches and direct injection into the mature OB avoids developmental expression and lineage bias commonly seen with genetic crosses, while also allowing wide-spread region- and cell type-specific targeting (94.14 ± 3.99% mCherry+, GFAP+ cells) (Figure 1B). For additional specificity, we intersectionally targeted mature astrocytes using conditional viral constructs driven by the astrocyte-specific GFAP promoter. Upon injection of AAV-GFAP-flex-mCherry into the OB, we observed mCherry in a large fraction of astrocytes, as verified by colabeling with GFAP. Even after 30 days post injection (dpi), we observed no off-target cellular expression in M/T cells (Tbx21), granule cells (calretinin), periglomerular cells (tyrosine hydroxylase, TH), or EPL interneurons (parvalbumin, PV) (Figure 1C). Aldh1L1 is also expressed in postnatal neural stem cells and transient amplifying cells within the subventricular zone (SVZ) and rostral migratory stream (RMS) (Alonso et al., 2008; Foo & Dougherty, 2013), which give rise to adult-born granule cells in the OB. Thus, genetically targeting astrocytes using an intersectional approach with conditionally expressed viruses under the GFAP promoter in *Aldh1L1-Cre* mice effectively labeled astrocytes with cell type specificity, thereby providing an effective means to selectively mark, monitor, and/or manipulate astrocytes within OB circuitry.

Astrocytes display odor response maps that overlap with mitral and tufted cells

To understand how astrocyte and neuronal activity is coordinated during sensory processing, we first sought to observe OB astrocyte activity compared to M/T cells in response to volatile odor stimuli. Towards this, we generated *Aldh1L1-Cre; Thy1-GCaMP3* double transgenic mice (RRID: IMSR_JAX:017893). These mice expressed the genetically-encoded calcium indicator (GECI) GCaMP3 in M/Ts, and Cre recombinase in astrocytes to facilitate

astrocyte-specific expression of the red-shifted genetically-encoded calcium indicator jRCaMP1a with injection of a conditional AAV (Dana et al., 2016) (Figure 2A). Simultaneous expression of GECIs with different emission wavelengths in two non-overlapping populations of cells allowed us to observe the activity of both neurons and astrocytes in response to odor stimulation through sequential imaging trials. To image odor responses, we visualized the entire dorsal OB by wide-field fluorescent imaging of the glomerular layer through thinned skull under anesthesia (Figure 2B). To evaluate odor response specificity, we differentially presented a panel of 4 odorants, each of which activated different sets of identifiable glomeruli on the dorsal surface of the OB (Figure 2C). Although odor-specific patterns of activation varied slightly between animals, general domains of M/T cell activation were reproducible, and similar to previous findings (Quast et al., 2017). Initially examining the response patterns of astrocytes, we observed that different odorants elicited unique spatial patterns of activation (Figure 2C). These findings were consistent with previous work indicating that astrocytes at glomeruli are activated by physiological odor-evoked stimuli (Otsu et al., 2014). By implementing automated maximum entry thresholding approaches, we generated binary activity maps from the previously described response maps. The binary activity maps of astrocytes revealed closely overlapping domains relative to the activation domains of M/T cells, as observed through sequential jRCaMP1a and GCaMP3 imaging ($63.87 \pm 20.91\%$ overlap of activated astrocyte domains in activated neuronal domains, n = 3 male and 2 female mice with 5 odors per mouse), respectively. These overlapping domains accounted for $50.99 \pm 22.31\%$ of astrocyte areas activated by odor stimulus. Examining the kinetics of both cell populations, the time to peak calcium responses in astrocytes occurred with similar timescales to odor-evoked responses in neurons (Figure 2D-E, $2.46s \pm 1.19s$ in astrocytes vs $1.68s \pm 0.15s$ in neurons; Student's T-test, p = 0.6642). However, decay times (from 90% to 30% of the peak amplitude) of astrocytic calcium signals were substantially slower (Figure 2F, $1.68s \pm 0.89s$ in neurons vs $3.12s \pm 1.30s$ in astrocytes; Student's T-test, $*p < 0.05$). However, it is possible that direct comparison of response dynamics between M/T cell and astrocyte responses may be skewed due to differences in kinetics between GCaMP and jRCaMP1a. Thus, we examined the kinetic differences between neuronal and astrocyte calcium responses in domains that overlap with and without the other population (Figure 2G). While neuronal response properties were unaffected by the presence or absence of astrocyte calcium responses, astrocyte calcium responses showed increased peak responses ($8.69 \pm 0.81\%$ in overlapping domains vs $6.03 \pm 1.90\%$ in astrocyte-only domains, Unpaired Student's t-test, $*p < 0.0210$) as well as decreased time to peak ($2.05 \pm 0.29s$ in overlapping domains vs $2.54 \pm 0.30s$ in astrocyte-only domains, Unpaired Student's t-test, $*p < 0.0292$) (Figure 2H).These data, detailing odor-specific patterning of astrocyte calcium signals, further substantiate previous findings that odors induce calcium transients in astrocytes within olfactory glomeruli (Otsu et al., 2014).

Astrocyte intracellular signaling modulates neuronal activity

Having established that astrocytes show stereotyped spatio-topographical calcium responses to olfactory stimuli, we next sought to determine whether manipulating astrocytic intracellular signaling influenced M/T cell responses. Using *Aldh1L1-Cre; Thy1-GCaMP3* double transgenic mice, we manipulated astrocyte intracellular signaling through selective

expression of inducible chemogenetic DREADDs (Armbruster, Li, Pausch, Herlitze, & Roth, 2007; Wulff & Arenkiel, 2012) (Figure 3A). Towards this, we injected a conditional AAV-GFAP-flex-hM3D-mCherry vector into *AldhL1-Cre; Thy1GCaMP3* mice (Figure 3B). Previous work has demonstrated that *in vivo* administration of Clozapine N-oxide (CNO) activates expressed hM3Dq reporters in astrocytes, which triggers robust calcium transients through modulation of the G_q pathway (Scofield et al., 2015; L. Yang, Qi, & Yang, 2015). To evaluate the consequences of astrocyte intracellular signaling onto M/T cell output, we imaged sensory maps of M/T cells in response to a panel of odorants in triplicate. We then performed IP injections of CNO (5 mg/kg in 200 μL saline) to activate hM3Dq, and imaged sensory maps of M/T cells again in the same OB (Figure 3C). At baseline, typical M/T cell sensory maps showed conserved and reproducible odorant specificity. Upon increasing astrocyte activity through CNO activation of hM3Dq-expressing astrocytes, we observed a decrease in odor-evoked M/T cell activity (Figure 3D-E. n = 5 male and 8 female mice; 2-way repeated measures ANOVA with Sidak's multiple comparison correction, $F_{(1, 36)} = 36.99$, main effect of group: $p < 0.0001$, group x odor interaction: $p = 0.7952$, multiple comparisons: $*p < 0.05$, t = 3.047; $**p < 0.01$, t = 3.481; $***p < 0.001$, t = 4.006). While sensory map patterns and temporal kinetics remained consistent, the observed decrease in M/T cell activity upon induction of astrocyte intracellular signaling suggested a role for astrocytes in M/T cell inhibition.

We next sought to determine if manipulating other astrocyte intracellular signaling pathways would produce different effects in Ca^{2+} activity in M/T cells. For this, we selectively targeted expression of hM4Di to astrocytes by again injecting GFAP-driven conditional hM4Di viral vectors into the bulbs of *Aldh1L1-Cre; Thy1-GCaMP3* mice. While CNO activation of hM3Dq induced signaling in astrocytes through the G_q pathway, CNO activation of hM4Di signals through $G_{i/o}$, and thus stimulated astrocyte intracellular signaling through a different pathway (Durkee et al., 2019). After allowing 2 weeks for hM4Di-mCherry expression, we imaged control odor response maps at baseline, and again after stimulating astrocyte activity with CNO injection. With $G_{i/o}$ DREADD-mediated stimulation of astrocyte activity, odor-evoked M/T cell activity was increased compared to baseline (Figure 3F-G. n = 5 male and 4 female mice; 2-way repeated measures ANOVA with Sidak's multiple comparison correction, $F_{(1, 24)} = 38.34$, main effect of group: $p < 0.0001$, group x odor interaction: $p = 0.7073$, multiple comparisons: $*p < 0.05$, t = 3.064; $**p < 0.01$, t = 3.436; $***p < 0.001$, t = 4.225). Again, no discernible changes in the shape and/or size of sensory response maps were observed. Collectively, these data indicate that astrocyte activity influences neuronal output during olfaction.

Local astrocyte signaling affects olfactory behavior

Given that astrocyte intracellular signaling modulates M/T cell responses in the OB, we next investigated whether astrocytes exert direct effects on olfactory behavior. Towards this, we bilaterally injected AAV-GFAP-flex-hM3Dq-mCherry or -hM4Di-mCherry into OBs of *Aldh1L1-Cre* mice to selectively manipulate astrocytes. After recovery, we trained mice to perform a Go/NoGo associated olfactory learning task (G. Liu et al., 2017), in which reward is associated with olfactory cues (Figure 4A). We then identified the odor detection threshold of these mice during active investigation by presenting a pair of odorants in a

descending-concentration series, and recording accuracy of performing the Go/No-Go task (Figure 4B). We found that mice accurately performed the task at concentrations at and above 10^{-5} (v/v) of both odorants used for training (n = 8 male and 8 female mice; 87.25 $\pm 6.61\%$ correct action). At a concentration of 10^{-6}, mice were challenged in accurately executing the task, but performed above chance (74.78 $\pm$ 11.40%). At concentrations of 10^{-7}, mice were unable to accurately perform the task, and behaved near chance (55.43 $\pm$ 10.30%), suggesting an inability to detect dilute odors. We then tested these concentrations again after IP injection of CNO (5 mg/kg) to induce astrocyte activity with either hM3Dq or hM4Di. We observed that at 10^{-5}, mice were still able to reliably detect the odors and accurately performed the task. Furthermore, at 10^{-7}, mice were still unable to detect these odors and failed at performing the task (Figure 4C, E). Interestingly, however, we observed that hM3Dq-induction of astrocyte activity, which corresponded to decreased neuronal activity, improved the accuracy near odor detection thresholds at 10^{-6} (Figure 4D). Conversely, hM4Di-induced astrocyte activity, led to decreased accuracy at this concentration. (Figure 4F). Together these data suggest that not only does astrocytic intracellular signaling onto or between M/T cells directly impact olfactory behavior, but the signaling pathway in astrocytes is important in determining the effect.

Discussion

Here we performed cell type-specific manipulations on astrocytes while imaging M/T cell olfactory response maps, and have begun to reveal important roles for astrocytes in direct modulation of sensory circuits. Combining genetic and viral manipulations with *in vivo* imaging methods, we found that astrocytes show odor response maps similar to M/T cells. Notably, we found that astrocytic intracellular signaling not only modulates activity levels of neurons, but also affects behavioral output in odor detection tasks. Together these data reveal functional roles for astrocytes in governing neuronal signaling properties, and support their direct involvement in sensory processing.

A major challenge in the field of glial biology has been the selective targeting of astrocytes in the adult brain. While neurons now have numerous cell type-specific Cre drivers that allow for heterogenous expression in similar regions or subtype-specific targeting, astrocytes not only lack such diverse drivers, but many typical astrocyte markers show dynamic and/or transient expression in neuronal stem cell populations. Here we introduce an approach to target astrocytes, while avoiding potentially overlapping expression in neuronal lineages. Towards this, we used the widespread astrocyte marker Aldh1L1 for genetic recombination, followed by canonical astrocyte marker GFAP for viral promoter expression. This provided a simple, intersectional approach for selectively targeting astrocytes while excluding neurons (Figure 1). Another key feature of this experimental approach is that stereotaxic viral targeting allows for adult- and region-specific manipulations. Notably, in cases where circuit-associated behavioral outputs span multiple regions, complementary use of combined viral approaches may allow for the dissection of regional contributions. Finally, given recent studies illustrating regional diversity of astrocytes (Chai et al., 2017; Morel et al., 2018), such reagents and approaches may be useful in dissecting the underlying functional diversity of astrocytes within diverse brain regions.

Although it is well appreciated that astrocytes play major roles in both synaptic assembly (Elmariah, Oh, Hughes, & Balice-gordon, 2005; Ullian, 2001), and synaptic physiology in the adult brain (Allen & Barres, 2009; Eroglu & Barres, 2010; Y. Yang, Higashimori, & Morel, 2013), our studies reveal a new role for astrocytes in the circuit modulation of sensory response maps within the OB. We show that odor-evoked physiological stimulation generated calcium responses in glomerular astrocytes with domains corresponding to odor input, resulting in a spatial map representation of odorants. Astrocytic calcium responses showed similar odor specificities and spatial constraints to M/T cell responses, suggesting coordinated, input-driven activity. However, it is important to note the differences in kinetics between the two GECIs used to monitor astrocytic calcium and neuronal calcium. Due to these differences, interpretation of relative rise and decay times may be distorted. The differences in astrocyte calcium response kinetics in domains with and without neuronal responses further suggest that astrocytes may have roles altered by neuronal activity. These data suggest an important role for astrocytic calcium-mediated mechanisms in modulating input circuit-specific olfactory responses. In astrocytes, calcium signaling has been implicated in many intracellular and extracellular functions, including but not limited to juxtacellular signaling, neurovascular coupling, changes in cell morphology, and gliotransmission (Araque et al., 2014; Haydon & Carmignoto, 2006; Nedergaard, Ransom, & Goldman, 2003; Stogsdill et al., 2017; Wang et al., 2006). Interestingly, the hotspots of odor-evoked astrocyte activity are approximately the size of glomeruli. Indeed, glomerular structures include astrocyte cell bodies residing along their periphery, with astrocytic processes enclosing neuropil in a central-synaptic subcompartment (Chao, Kasa, & Wolff, 1997). Astrocytes associated with the same glomerulus form a large multicellular syncytium through gap junctions located at their perisynaptic processes (Fujii, Maekawa, & Morita, 2017), which can lead to unitary functional glial network responses characterized by calcium waves that propagate through astrocyte clusters within odor-activated glomeruli (Hirase, Qian, Barthó, & Buzsáki, 2004; Roux, Benchenane, Rothstein, Bonvento, & Giaume, 2011). Overall synchrony between astrocyte anatomy, spatial localization, and range of functions may coordinate effects onto neurons at the cellular level through neuron-astrocyte interactions, which then manifests into circuit-level phenomena.

Inhibition is highly relevant within sensory circuits, playing an integral role in the brain's ability to adapt, learn, and discern similar sensory stimuli. For example, it has been previously shown that inhibitory neurons directly influence phases of enhanced plasticity during critical periods (Hensch, 2005). Inhibitory granule cells are the most numerous cell type in the OB, and are thought to provide lateral inhibition for contrast enhancement (Lledo, Saghatelyan, & Lemasson, 2004; Shepherd, Chen, Willhite, Migliore, & Greer, 2007). Intriguingly, we found that stimulation of astrocyte intracellular signaling through hM3D led to an inhibition in neuronal activity, suggesting an additional mechanism for inhibition in the OB. This astrocyte-derived inhibition could be facilitated directly onto M/T cells via inhibitory gliotransmitters such as GABA (Yoon & Lee, 2014), through calcium-dependent potassium buffering (Weiss et al., 2019), through modulation of synaptic transmission from presynaptic inputs (Martin-Fernandez et al., 2017), or through inhibition of M/T cells, either through astrocyte-derived excitation of inhibitory interneurons in the OB or presynaptic modulation of olfactory sensory neurons (Petzold, Hagiwara, & Murthy,

2009). However, use of DREADD manipulations does not exclusively modulate Ca^{2+} activity. Given that DREADD technologies are derived from GPCRs, a number of parallel and intersecting pathways downstream of these GPCR activities may be effected to ultimately result in the phenomena described in this study.

Interestingly, behavioral results that show increased sensory performance are counterintuitive given that imaging data with hM3Dq-induced astrocyte intracellular signaling led to a decrease in neuronal activity. We speculate that although this manipulation results in decreased neuronal activity, this could lead to an increase in the signal-to-noise ratio of odor-driven neuronal activity, and thus lend to enhanced detection of odors over ambient background. Furthermore, these effects are only seen at odor concentrations near detection thresholds (10^{-6}), suggesting that the contributions of astrocytes are subtle and are not solely sufficient to completely override neuronal signaling. While the DREADDs have been commonly used, it is important to note the metabolic products of CNO could also have off-target effects on behavioral assays (Manvich et al., 2018). Such potential off-target effects have been shown to be dose-dependent, ranging from 1-20 mg/kg- with high variability in individual subjects. As such, we cannot completely rule out the affects of interoceptive effects from CNO on this behavioral task. A further limitation to our experimental methods is the broad manipulation of astrocytes in the OB, rather than only the astrocytes driven by odor-specific input. Future development of astrocyte-specific technologies could facilitate experiments examining input- or circuit-specific modulation of astrocytes as has been done in neurons (X. Liu et al., 2012; Sakurai et al., 2016).

We propose a model in which astrocyte signaling, responding to odor-evoked physiological stimuli, leads to inhibition of M/T cells. There are many potential candidates for gliotransmitters that may govern this process. For example, previous studies have reported that ATP derived from astrocytes leads to local suppression of excitatory synaptic transmission through the extracellular conversion to adenosine, followed by subsequent binding to adenosine A1 receptors (Haydon & Carmignoto, 2006; Pascual, 2005; L. Yang et al., 2015) or purinergic receptors (Lohr, Grosche, Reichenbach, & Hirnet, 2014). The diffusion and conversion of extracellular ATP to adenosine could account for widespread, domain-specific inhibition. Alternatively, glutamatergic activation of inhibitory cells could also lead to lateral inhibition of M/Ts (Abraham et al., 2010; Giridhar, Doiron, & Urban, 2011; Margrie, Sakmann, & Urban, 2001; Urban & Sakmann, 2002). Finally, given the expanding repertoire of gliotransmitters, the ability of astrocytes to respond to different patterns of neuronal activity with distinct gliotransmitter release (Covelo & Araque, 2018) further increases the complexity of how astrocytes can influence neuronal circuits.

While our approach targets astrocytes in an unbiased manner, it doesn't take into account the potential of different astrocyte subpopulations (Chai et al., 2017; John Lin et al., 2017; Morel et al., 2017), which may affect neurons in diverse ways. Additionally, complex patterns of intracellular calcium elevations (Bindocci et al., 2017) may lead to different downstream outputs from astrocytes. Astrocytes display localized calcium responses to different neuronal stimuli (Bernardinelli et al., 2011), and coupled with multiple astrocytic release processes dependent on v-SNARE proteins (Schwarz, Zhao, Kirchhoff, & Bruns, 2017) at the multitude of processes and leaflets present in complex astrocyte morphology,

we cannot rule out the possibility that multiple gliotransmitters within specific astrocyte processes onto different neuronal populations coordinate distinct odor-evoked neuronal responses. Future experiments examining the detailed mechanisms by which astrocytes can affect neuronal sensory systems will be crucial in understanding the extent of processing involved in sensory circuits. Furthermore, although we do not observe any sex-specific differences, we cannot completely rule this out due to the use of both sexes contributing to all experiments and data. While we assayed these phenomena across multiple odorants, the analyses were also limited by the low number of animals.

Taken together, our experiments build upon our evolving understanding of astrocyte-neuron interactions. In particular, that within sensory systems astrocytes play important functional roles in regulating the integration of input in a multidimensional system. We found that manipulation of astrocytes can lead to changes in neuronal activity patterns, resulting in alterations to odor detection thresholds and odor discrimination. Overall, our study reinforces the importance of examining interactions between multiple cell types toward unraveling how these interactions contribute towards sensory circuit function. To fully understand the complexity of how the brain shapes behavior, further investigation into glia subtypes and their interactions with neurons is imperative for processing the wide array of inputs into neuronal circuits.

Acknowledgements

References

Abraham NM, Egger V, Shimshek DR, Renden R, Fukunaga I, Sprengel R, … Kuner T (2010). Synaptic Inhibition in the Olfactory Bulb Accelerates Odor Discrimination in Mice. Neuron, 65(3), 399–411. 10.1016/j.neuron.2010.01.009 [PubMed: 20159452]

Allen NJ, & Barres BA (2009). Neuroscience: Glia - more than just brain glue. Nature, Vol. 457, pp. 675–677. 10.1038/457675a [PubMed: 19194443]

Alonso M, Ortega-Perez I, Grubb MS, Bourgeois J-P, Charneau P, & Lledo P-M (2008). Turning Astrocytes from the Rostral Migratory Stream into Neurons: A Role for the Olfactory Sensory Organ. Journal of Neuroscience, 28(43), 11089–11102. 10.1523/JNEUROSCI.3713-08.2008 [PubMed: 18945916]

Amédée T, Robert A, & Coles JA (1997). Potassium homeostasis and glial energy metabolism. GLIA, 21(1), 46–55. 10.1002/(SICI)1098-1136(199709)21:1<46::AID-GLIA5>3.0.CO;2-# [PubMed: 9298846]

Araque A, Carmignoto G, Haydon PG, Oliet SHR, Robitaille R, & Volterra A (2014). Gliotransmitters travel in time and space. Neuron, 81(4), 728–739. 10.1016/j.neuron.2014.02.007 [PubMed: 24559669]

Armbruster BN, Li X, Pausch MH, Herlitze S, & Roth BL (2007). Evolving the lock to fit the key to create a family of G protein-coupled receptors potently activated by an inert ligand. Proceedings of the National Academy of Sciences, 104(12), 5163–5168. 10.1073/pnas.0700293104

Bergles DE, & Jahr CE (1998). Glial contribution to glutamate uptake at Schaffer collateral-commissural synapses in the hippocampus. The Journal of Neuroscience : The Official Journal of the Society for Neuroscience, 18(19), 7709–7716. Retrieved from http://www.ncbi.nlm.nih.gov/pubmed/9742141 [PubMed: 9742141]

Bernardinelli Y, Salmon C, Jones EV, Farmer WT, Stellwagen D, & Murai KK (2011). Astrocytes Display Complex and Localized Calcium Responses to Single-Neuron Stimulation in the Hippocampus. Journal of Neuroscience, 31(24), 8905–8919. 10.1523/JNEUROSCI.6341-10.2011 [PubMed: 21677174]

Bindocci E, Savtchouk I, Liaudet N, Becker D, Carriero G, & Volterra A (2017). Three-dimensional Ca^{2+} imaging advances understanding of astrocyte biology. Science, 356(6339), eaai8185. 10.1126/science.aai8185 [PubMed: 28522470]

Bordey a, Hablitz JJ, & Sontheimer H (2000). Reactive astrocytes show enhanced inwardly rectifying K+ currents in situ. Neuroreport, 11(14), 3151–3155. 10.1097/00001756-200009280-00022 [PubMed: 11043540]

Cahoy JD, Emery B, Kaushal A, Foo LC, Zamanian JL, Christopherson KS, … Barres BA (2008). A Transcriptome Database for Astrocytes, Neurons, and Oligodendrocytes: A New Resource for Understanding Brain Development and Function. Journal of Neuroscience, 28(1), 264–278. 10.1523/JNEUROSCI.4178-07.2008 [PubMed: 18171944]

Cang J, & Feldheim DA (2013). Developmental Mechanisms of Topographic Map Formation and Alignment. Annual Review of Neuroscience, 36(1), 51–77. 10.1146/annurev-neuro-062012-170341

Chai H, Diaz-Castro B, Shigetomi E, Monte E, Octeau JC, Yu X, … Khakh BS (2017). Neural Circuit-Specialized Astrocytes: Transcriptomic, Proteomic, Morphological, and Functional Evidence. Neuron, 95(3), 531–549.e9. 10.1016/j.neuron.2017.06.029 [PubMed: 28712653]

Chao TI, Kasa P, & Wolff JR (1997). Distribution of astroglia in glomeruli of the rat main olfactory bulb: Exclusion from the sensory subcompartment of neuropil. Journal of Comparative Neurology, 388(2), 191–210. 10.1002/(SICI)1096-9861(19971117)388:2<191::AID-CNE2>3.0.CO;2-X

Covelo A, & Araque A (2018). Neuronal activity determines distinct gliotransmitter release from a single astrocyte. ELife. 10.7554/elife.32237

Dana H, Mohar B, Sun Y, Narayan S, Gordus A, Hasseman JP, … Kim DS (2016). Sensitive red protein calcium indicators for imaging neural activity. ELife, 5(32016). 10.7554/eLife.12727

Durkee CA, Covelo A, Lines J, Kofuji P, Aguilar J, & Araque A (2019). G i/o protein-coupled receptors inhibit neurons but activate astrocytes and stimulate gliotransmission. GLIA. 10.1002/glia.23589

Elmariah SB, Oh EJ, Hughes EG, & Balice-gordon RJ (2005). Astrocytes Regulate Inhibitory Synapse Formation via Trk- Mediated Modulation of Postsynaptic GABA A Receptors. Differences, 25(14), 3638–3650. 10.1523/JNEUROSCI.3980-04.2005

Eroglu C, & Barres BA (2010). Regulation of synaptic connectivity by glia. Nature, 468(7321), 223–231. 10.1038/nature09612 [PubMed: 21068831]

Fields RD, Woo DH, & Basser PJ (2015). Glial regulation of the neuronal connectome through local and long-distant communication. Neuron, 86(2), 374–386. 10.1016/j.neuron.2015.01.014 [PubMed: 25905811]

Foo LC, & Dougherty JD (2013). Aldh1L1 is Expressed by Postnatal Neural Stem Cells In Vivo. GLIA, 61(9), 1533–1541. 10.1002/glia.22539 [PubMed: 23836537]

Freeman MR (2006). Sculpting the nervous system: Glial control of neuronal development. Current Opinion in Neurobiology. 10.1016/j.conb.2005.12.004

Fujii Y, Maekawa S, & Morita M (2017). Astrocyte calcium waves propagate proximally by gap junction and distally by extracellular diffusion of ATP released from volume-regulated anion channels. Scientific Reports, 7(1). 10.1038/s41598-017-13243-0

Giridhar S, Doiron B, & Urban NN (2011). Timescale-dependent shaping of correlation by olfactory bulb lateral inhibition. Proceedings of the National Academy of Sciences, 108(14), 5843–5848. 10.1073/pnas.1015165108

Hanson E, Armbruster M, Cantu D, Andresen L, Taylor A, Danbolt NC, & Dulla CG (2015). Astrocytic glutamate uptake is slow and does not limit neuronal NMDA receptor activation in the neonatal neocortex. GLIA, 63(10), 1784–1796. 10.1002/glia.22844 [PubMed: 25914127]

Haydon PG, & Carmignoto G (2006). Astrocyte Control of Synaptic Transmission and Neurovascular Coupling. Physiological Reviews, 86(3), 1009–1031. 10.1152/physrev.00049.2005 [PubMed: 16816144]

Hensch TK (2005). Critical period plasticity in local cortical circuits. Nature Reviews Neuroscience, Vol. 6, pp. 877–888. 10.1038/nrn1787 [PubMed: 16261181]

Higashimori H, & Sontheimer H (2007). Role of Kir4.1 channels in growth control of glia. GLIA, 55(16), 1668–1679. 10.1002/glia.20574 [PubMed: 17876807]

Hirase H, Qian L, Barthó P, & Buzsáki G (2004). Calcium dynamics of cortical astrocytic networks in vivo. PLoS Biology, 2(4). 10.1371/journal.pbio.0020096

John Lin CC, Yu K, Hatcher A, Huang TW, Lee HK, Carlson J, … Deneen B (2017). Identification of diverse astrocyte populations and their malignant analogs. Nature Neuroscience, 20(3), 396–405. 10.1038/nn.4493 [PubMed: 28166219]

Lemke G (2002). Glial Control of Neuronal Development. Annual Review of Neuroscience. 10.1146/annurev.neuro.24.1.87

Liu G, McClard C, Tepe B, Swanson J, Pekarek B, Panneerselvam S, & Arenkiel B (2017). Olfactory Cued Learning Paradigm. BIO-PROTOCOL, 7(9). 10.21769/BioProtoc.2251

Liu X, Ramirez S, Pang PT, Puryear CB, Govindarajan A, Deisseroth K, & Tonegawa S (2012). Optogenetic stimulation of a hippocampal engram activates fear memory recall. Nature. 10.1038/nature11028

Lledo P-M, Saghatelyan A, & Lemasson M (2004). Inhibitory interneurons in the olfactory bulb: from development to function. The Neuroscientist : A Review Journal Bringing Neurobiology, Neurology and Psychiatry, 10(4), 292–303. 10.1177/1073858404263460

Lohr C, Grosche A, Reichenbach A, & Hirnet D (2014). Purinergic neuron-glia interactions in sensory systems. Pflugers Archiv European Journal of Physiology, Vol. 466, pp. 1859–1872. 10.1007/s00424-014-1510-6 [PubMed: 24705940]

Ma DK, Ming GL, & Song H (2005). Glial influences on neural stem cell development: Cellular niches for adult neurogenesis. Current Opinion in Neurobiology. 10.1016/j.conb.2005.08.003

Magistretti PJ (2006). Neuron-glia metabolic coupling and plasticity. Journal of Experimental Biology, 209(12), 2304–2311. 10.1242/jeb.02208

Manvich DF, Webster KA, Foster SL, Farrell MS, Ritchie JC, Porter JH, & Weinshenker D (2018). The DREADD agonist clozapine N-oxide (CNO) is reverse-metabolized to clozapine and produces clozapine-like interoceptive stimulus effects in rats and mice. Scientific Reports. 10.1038/s41598-018-22116-z

Margrie TW, Sakmann B, & Urban NN (2001). Action potential propagation in mitral cell lateral dendrites is decremental and controls recurrent and lateral inhibition in the mammalian olfactory bulb. Proceedings of the National Academy of Sciences of the United States of America, 98(1), 319–324. 10.1073/pnas.98.1.319 [PubMed: 11120888]

Martin-Fernandez M, Jamison S, Robin LM, Zhao Z, Martin ED, Aguilar J, … Araque A (2017). Synapse-specific astrocyte gating of amygdala-related behavior. Nature Neuroscience. 10.1038/nn.4649

Martinez VK, Saldana-Morales F, Sun JJ, Zhu PJ, Costa-Mattioli M, & Ray RS (2019). Off-target effects of clozapine-N-oxide on the chemosensory reflex are masked by high stress levels. Frontiers in Physiology. 10.3389/fphys.2019.00521

Morel L, Men Y, Chiang MSR, Tian Y, Jin S, Yelick J, … Yang Y (2018). Intracortical astrocyte subpopulations defined by astrocyte reporter Mice in the adult brain. GLIA. 10.1002/glia.23545

Morel L, Ming X, Chiang SR, Higashimori H, Shoneye T, Iyer LK, … Yang XY (2017). Molecular and Functional Properties of Regional Astrocytes in the Adult Brain. The Journal of Neuroscience. 10.1523/JNEUROSCI.3956-16.2017

Nedergaard M, Ransom B, & Goldman SA (2003). New roles for astrocytes: Redefining the functional architecture of the brain. Trends in Neurosciences, 26(10), 523–530. 10.1016/j.tins.2003.08.008 [PubMed: 14522144]

Newman GC, Hospod FE, Qi H, Patel H, Trowbridge SD, & Patlak CS (1995). Effects of K+, pH and glutamate on 45Ca kinetics in hippocampal brain slices. Journal of Neuroscience Methods, 59(1), 111–120. 10.1016/0165-0270(94)00201-Q [PubMed: 7475241]

Otsu Y, Couchman K, Lyons DG, Collot M, Agarwal A, Mallet J-M, … Charpak S (2014). Calcium dynamics in astrocyte processes during neurovascular coupling. Nature Neuroscience, 18(2), 210–218. 10.1038/nn.3906 [PubMed: 25531572]

Pascual O (2005). Astrocytic Purinergic Signaling Coordinates Synaptic Networks. Science, 310(5745), 113–116. 10.1126/science.1116916 [PubMed: 16210541]

Petzold GC, Hagiwara A, & Murthy VN (2009). Serotonergic modulation of odor input to the mammalian olfactory bulb. Nature Neuroscience. 10.1038/nn.2335

Quast KB, Ung K, Froudarakis E, Huang L, Herman I, Addison AP, … Arenkiel BR (2017). Developmental broadening of inhibitory sensory maps. Nature Neuroscience, 20(2), 189–199. 10.1038/nn.4467 [PubMed: 28024159]

Robel S, & Sontheimer H (2015). Glia as drivers of abnormal neuronal activity. Nature Neuroscience, 19(1), 28–33. 10.1038/nn.4184

Roux L, Benchenane K, Rothstein JD, Bonvento G, & Giaume C (2011). Plasticity of astroglial networks in olfactory glomeruli. Proceedings of the National Academy of Sciences, 108(45), 18442–18446. 10.1073/pnas.1107386108

Sakurai K, Zhao S, Takatoh J, Rodriguez E, Lu J, Leavitt AD, … Wang F (2016). Capturing and Manipulating Activated Neuronal Ensembles with CANE Delineates a Hypothalamic Social-Fear Circuit. Neuron, 92(4), 739–753. 10.1016/j.neuron.2016.10.015 [PubMed: 27974160]

Schousboe A (2018). Metabolic signaling in the brain and the role of astrocytes in control of glutamate and GABA neurotransmission. Neuroscience Letters. 10.1016/j.neulet.2018.01.038

Schwarz Y, Zhao N, Kirchhoff F, & Bruns D (2017). Astrocytes control synaptic strength by two distinct v-SNARE-dependent release pathways. Nature Neuroscience, (9). 10.1038/nn.4647

Scofield MD, Boger HA, Smith RJ, Li H, Haydon PG, & Kalivas PW (2015). Gq-DREADD selectively initiates glial glutamate release and inhibits cue-induced cocaine seeking. Biological Psychiatry, 78(7), 441–451. 10.1016/j.biopsych.2015.02.016 [PubMed: 25861696]

Shepherd GM, Chen WR, Willhite D, Migliore M, & Greer CA (2007). The olfactory granule cell: From classical enigma to central role in olfactory processing. Brain Research Reviews, Vol. 55, pp. 373–382. 10.1016/j.brainresrev.2007.03.005 [PubMed: 17434592]

Sofroniew MV, & Vinters HV (2010). Astrocytes: Biology and pathology. Acta Neuropathologica, Vol. 119, pp. 7–35. 10.1007/s00401-009-0619-8 [PubMed: 20012068]

Stogsdill JA, Ramirez J, Liu D, Kim YH, Baldwin KT, Enustun E, … Eroglu C (2017). Astrocytic neuroligins control astrocyte morphogenesis and synaptogenesis. Nature, 551(7679), 192–197. 10.1038/nature24638 [PubMed: 29120426]

Ullian EM (2001). Control of Synapse Number by Glia. Science, 291(5504), 657–661. 10.1126/science.291.5504.657 [PubMed: 11158678]

Urban NN, & Sakmann B (2002). Reciprocal intraglomerular excitation and intra- and interglomerular lateral inhibition between mouse olfactory bulb mitral cells. Journal of Physiology, 542(2), 355–367. 10.1113/jphysiol.2001.013491

Vargova L, & Sykova E (2009). Astrocytes in control of the biophysical properties of extracellular space. In Astrocytes in (Patho)Physiology of the Nervous System (pp. 225–250). 10.1007/978-0-387-79492-1_9

Wang X, Lou N, Xu Q, Tian G-F, Peng WG, Han X, … Nedergaard M (2006). Astrocytic Ca2+ signaling evoked by sensory stimulation in vivo. Nature Neuroscience, 9(6), 816–823. 10.1038/nn1703 [PubMed: 16699507]

Weiss S, Melom JE, Ormerod KG, Zhang YV, & Littleton JT (2019). Glial Ca2+ signaling links endocytosis to K+ buffering around neuronal somas to regulate excitability. ELife. 10.7554/eLife.44186

Wulff P, & Arenkiel BR (2012). Chemical genetics: Receptor-ligand pairs for rapid manipulation of neuronal activity. Current Opinion in Neurobiology, Vol. 22, pp. 54–60. 10.1016/j.conb.2011.10.008 [PubMed: 22119143]

Yang L, Qi Y, & Yang Y (2015). Astrocytes Control Food Intake by Inhibiting AGRP Neuron Activity via Adenosine A$_1$ Receptors. Cell Reports, 11(5), 798–807. 10.1016/j.celrep.2015.04.002 [PubMed: 25921535]

Yang Y, Higashimori H, & Morel L (2013). Developmental maturation of astrocytes and pathogenesis of neurodevelopmental disorders. Journal of Neurodevelopmental Disorders, 5(1), 22. 10.1186/1866-1955-5-22 [PubMed: 23988237]

Yoon B-E, & Lee CJ (2014). GABA as a rising gliotransmitter. Frontiers in Neural Circuits. 10.3389/fncir.2014.00141

Significance

Sensory systems are required for processing information from the external environment. Loss or damage to sensory systems dramatically complicates quality of life. Understanding circuit mechanisms that contribute towards sensory processing is important towards developing therapeutics to prevent sensory loss- or restore perception. Here we utilized the mouse olfactory system as a model to identify contributions of astrocytes towards sensory processing.
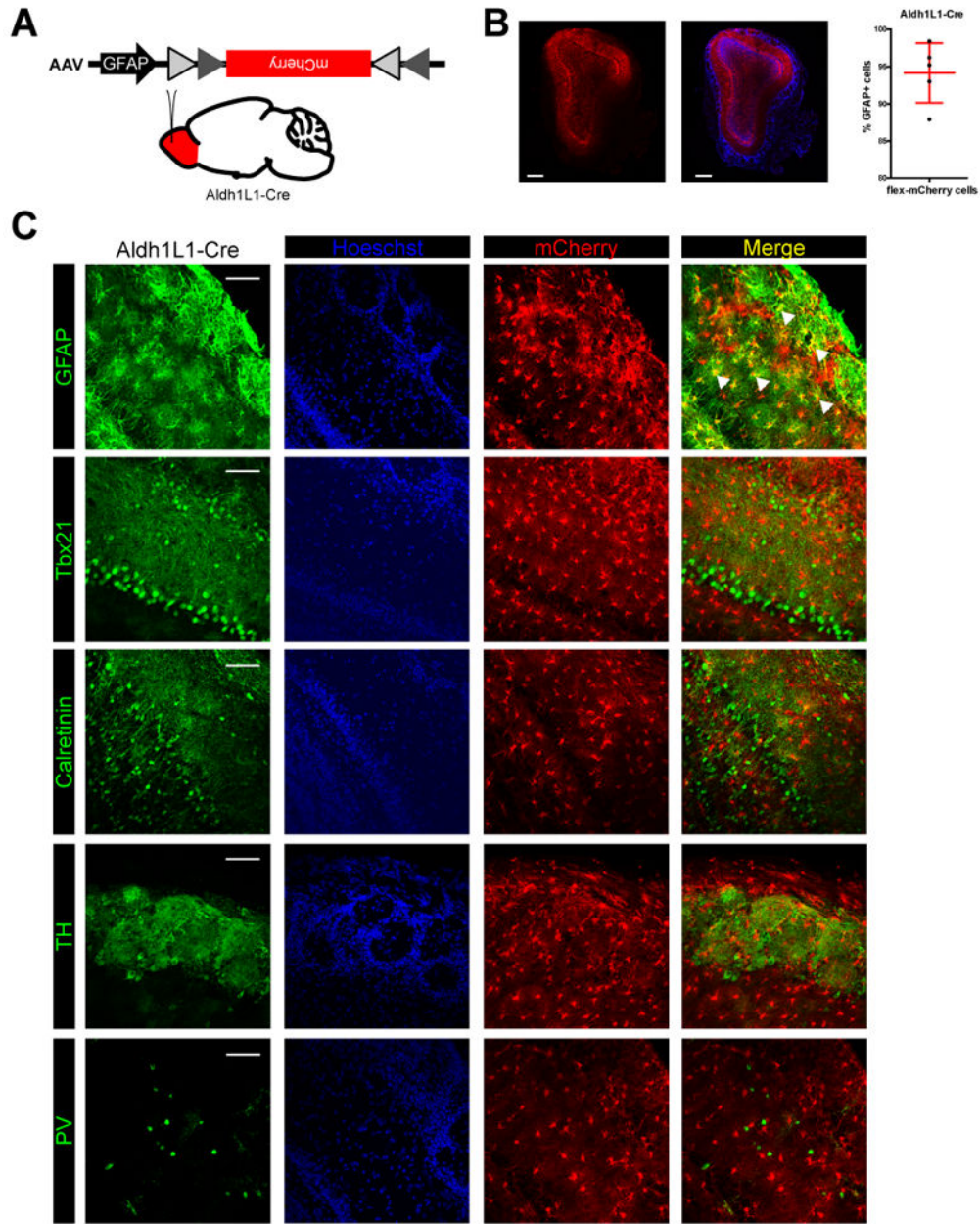
Figure 1. Genetically targeted astrocytes in the adult olfactory bulb does not colabel with neurons.

(A) Schematic of genetically targeting astrocytes in the adult olfactory bulb with viral constructs driven by the GFAP promoter.

(B) Coronal section showing widespread expression of virally-transduced mCherry in astrocytes throughout the OB. Scale bar, 300 μm. Graph showing the percentage of Aldh1L1-Cre astrocytes infected with AAV-GFAP-flex-mCherry that were also GFAP+. N = 2 male and 2 female mice.

(C) Coronal sections of the OB show that mCherry-expressing cells (astrocytes) do not colocalize with periglomerular cells (tyrosine hydroxylase, TH) or EPL interneurons (parvalbumin, PV). Scale bar, 100 μm.
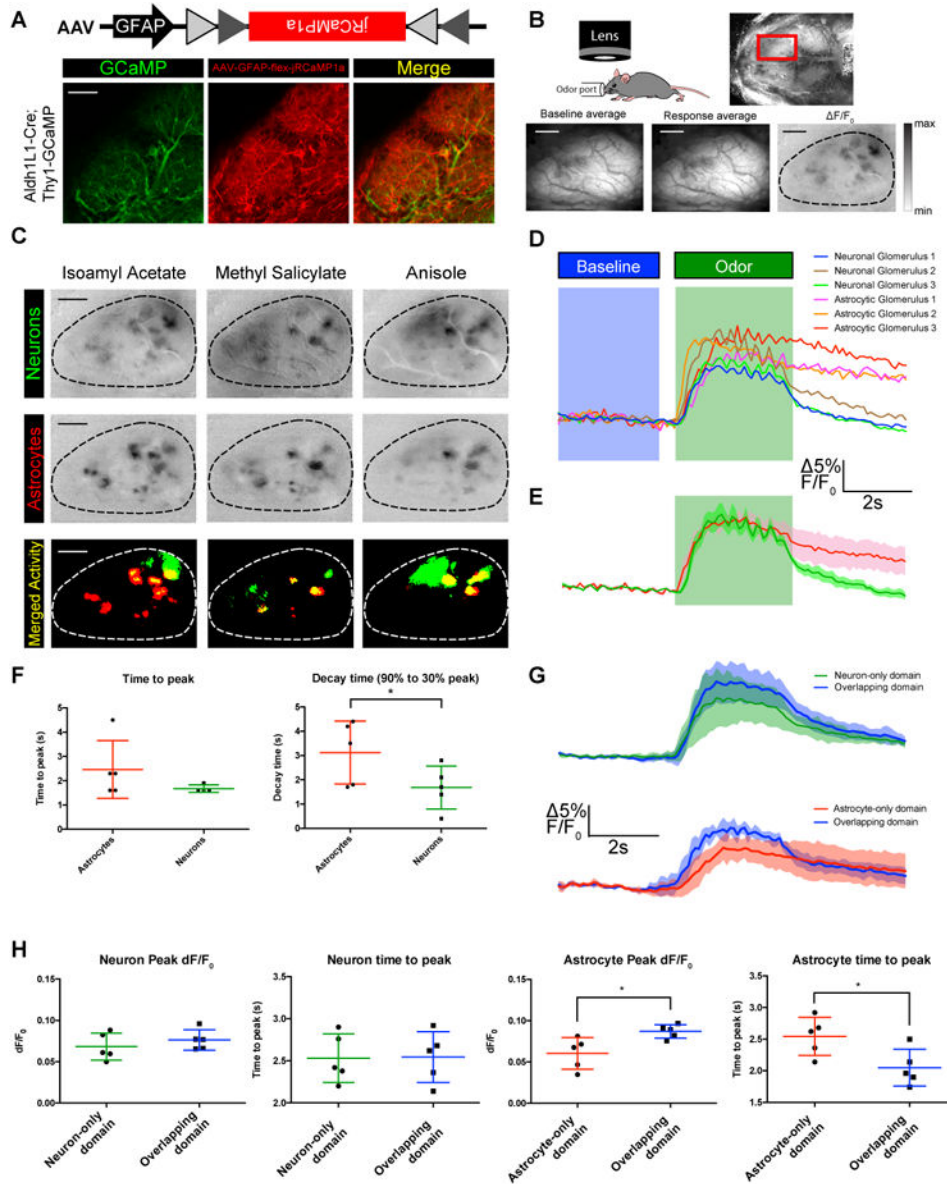
Figure 2. Astrocyte odor-evoked sensory maps visualized through calcium imaging overlap with M/T cells.

(A) Schematic of Cre-dependent AAV (top). Coronal section of mouse olfactory bulb showed expression of GCaMP in M/T cells (bottom left) and jRCaMP1a in astrocytes (bottom center) with no colocalization (merge, bottom right) in the glomerular layer. Scale bar, 30 μm.

(B) Schematic of widefield imaging of anesthetized mouse during odor presentation. Imaging of GCaMP3 above the thinned skull over the mouse OB allows for generation of neuronal olfactory sensory maps based on baseline subtraction of GCaMP3 signal. Scale bar, 500 μm.

(C) Example response maps to three different odorants. Response maps for M/T cells expressing GCaMP (top) and astrocytes expressing jRCaMP1a (middle) showed overlapping expression (bottom). n = 3 male and 2 female mice

(D) Example normalized traces of ROIs around glomeruli depicting temporal kinetics of fluorescent response in neurons and astrocytes to odorants before, during, and after odor delivery.

(E) Average normalized traces of temporal kinetics of fluorescent responses in neurons and astrocytes to odorants before, during, and after odor delivery.

(F) Quantification of (E). During odor delivery, there is no change in time to peak between neurons and astrocytes. However, the decay-time (from 90% to 30% peak) shows a significant increase in decay of calcium signaling in astrocytes compared to neurons. n = 3 male and 2 female mice

(G) Average normalized traces of temporal kinetics of fluorescent responses before, during, and after odor delivery in neurons with and without astrocyte responses (top) and in astrocytes with and without neuronal responses (bottom).

(H) Quantification of (G). During odor delivery, there is no change in time to peak or max response between neurons with and without astrocyte domains. However, max response in astrocytes was increased and time to peak was decreased in domains overlapping with neuronal activity.
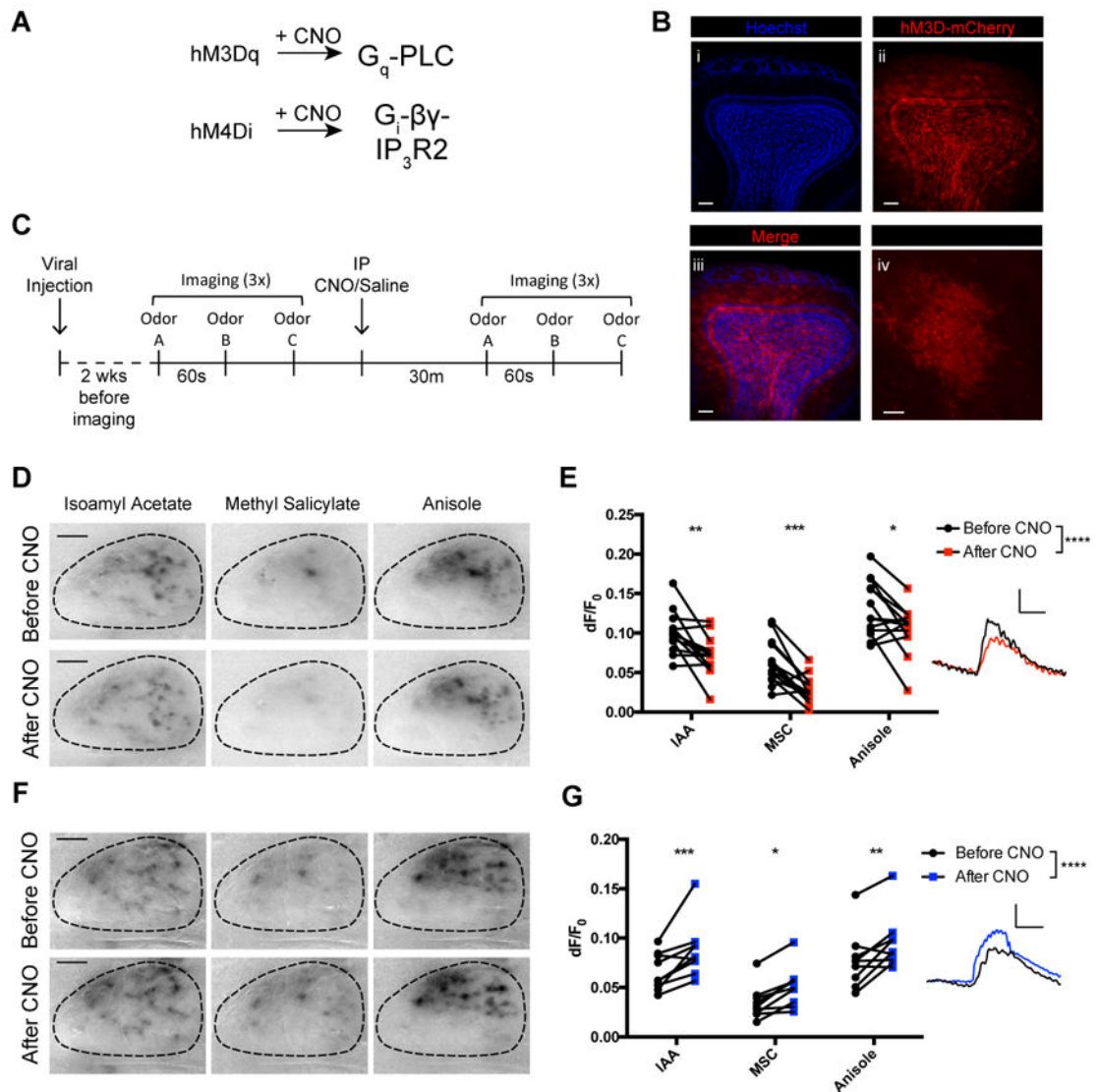
Figure 3. DREADD-induced astrocyte activity inhibited neuronal responses.

(A) hM3Dq or hM4Di DREADDs, expressed in astrocytes and activated by CNO, modulates calcium signaling.

(B) Representative images of viral hM3D-mCherry expression in astrocytes in the OB. Scale bar, 100 μm. i) Hoeschst stain of coronal OB section. ii) Viral hM3D-mCherry expression in OB astrocytes. iii) Merge of i) and ii). iv) High magnification of membrane-bound hM3D-mCherry in OB astrocyte. Scale bar, 5 μm.

(C) Schematic of imaging protocol. Sensory maps of odorants were imaged in one OB in triplicate before and after CNO or Saline injection.
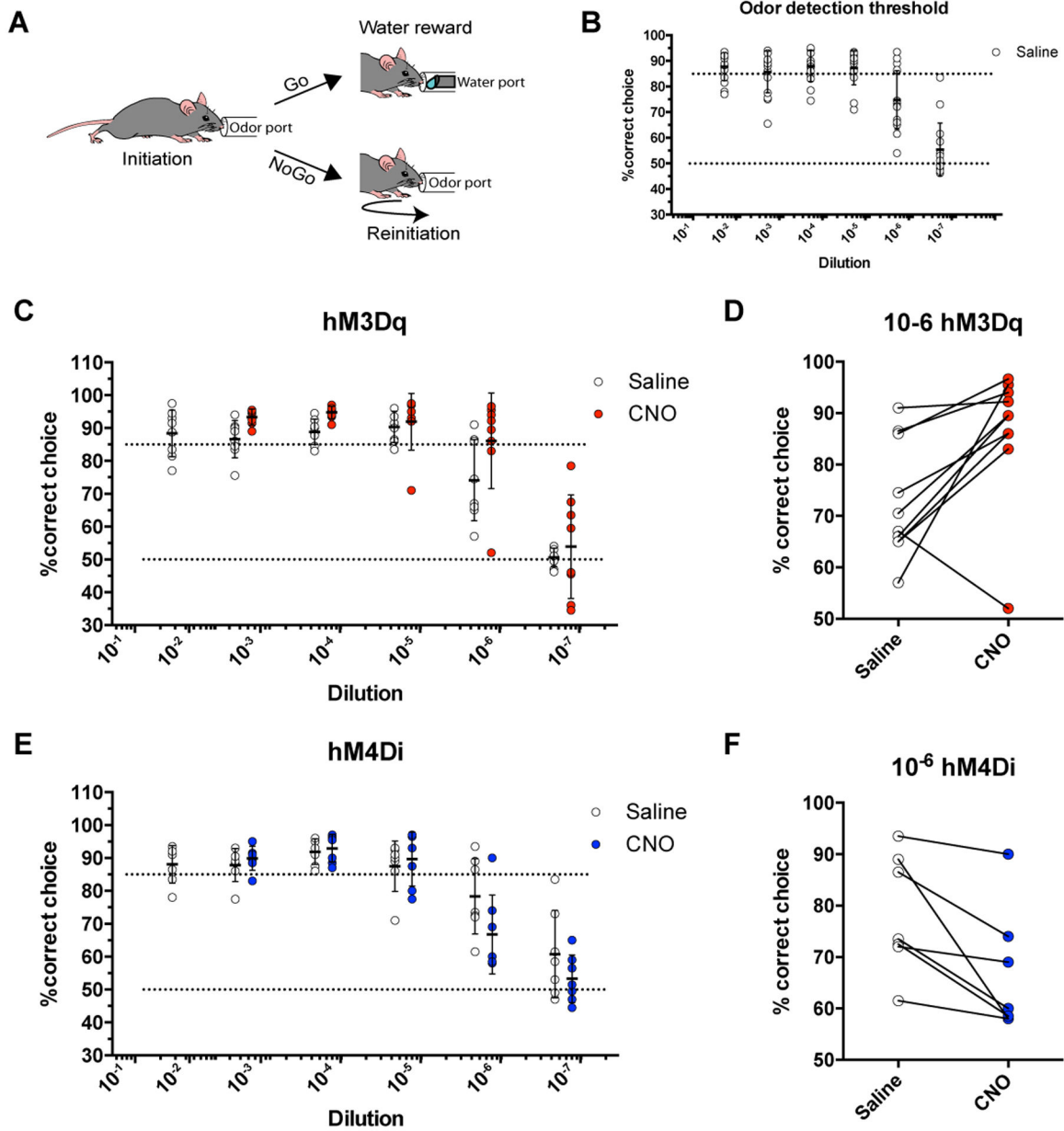
(D) Sensory maps of mitral cells before (top) and after (bottom) CNO induction of hM3D in astrocytes.

(E) Graph of change in fluorescence in neurons before and after injection of CNO to stimulate astrocyte activity. After CNO administration, neurons showed a decrease in fluorescence in activated regions during odorant presentation (n = 5 male and 8 female

mice). Example trace (inset) reveals similar temporal kinetics for rise and decay during and after stimulus presentation, respectively.

(F) Sensory maps of mitral cells before (top) and after (bottom) CNO induction of hM4D in astrocytes.

(G) Graph of change in fluorescence in neurons before and after injection of CNO to inhibit astrocyte activity. After CNO administration, neurons showed an increase in fluorescence in activated regions during odorant presentation (n = 5 male and 4 female mice). Example trace (inset) reveals similar temporal kinetics for rice and decay during and after stimulus presentation, respectively.

Figure 4. Astrocytic calcium directly affected olfactory behavior

(A) Schematic of olfactory-associated Go-NoGo behavioral task.

(B) Odor detection curve in n = 8 male and 8 female control mice. Mice were reliably able to detect odors at 10^{-5} (v/v) and performed approximately at chance at 10^{-7}.

(C) Odor detection curve in n = 4 male and 6 female mice expressing hM3Dq. Black lines represent the detection curve before CNO treatment while red lines represent odor detection curve after CNO treatment.

(D) At the concentration in which performance was most sensitive (10^{-6}), G_q-mediated astrocyte activity increased performance in detecting and responding to odorant cues. n = 4 male and 6 female mice. *p = 0.0149, Paired Student's t-test.

(E) Odor detection curve in n = 4 male and 3 female mice expressing hM4Di. Black lines represent the detection curve before CNO treatment while red lines represent odor detection curve after CNO treatment.

(F) At the concentration in which performance was most sensitive (10^{-6}), G_i-mediated astrocyte activity decreased performance in detecting and responding to odorant cues. n = 4 male and 3 female mice. *p = 0.0216, Paired Student's t-test.

Antibody name	Structure and host	Catalog number	Concentration	RRID
Anti-GFAP antibody	IgG, Polyclonal antibody, Host rabbit	DAKO Z0034	1:1000	AB_2811722
Anti-Tbx21 antibody	IgG, Polyclonal antibody, Host rabbit	NA	1:500	NA
Anti-calretinin antibody	IgG, Polyclonal antibody, Host mouse	Millipore MAB1572	1:1500	AB_94259
Anti-parvalbumin antibody	IgG, Polyclonal antibody, Host mouse	Millipore MAB1572	1:3000	AB_2174013
Alexa-488 anti-rabbit antibody	IgG, Polyclonal antibody, Host goat	Thermofisher A10040	1:500	AB_2534016
Alexa-488 anti-mouse antibody	IgG, Polyclonal antibody, Host goat	Thermofisher A11001	1:500	AB_2534069
Anti-TH antibody	IgG, Polyclonal antibody, Host rabbit	Millipore Ab152	1:2000	AB_390204